crystals

MDPI

Review

Role of the Potential Barrier in the Electrical Performance of the Graphene/SiC Interface

Ivan Shtepliuk [1,*], Tihomir Iakimov [1], Volodymyr Khranovskyy [1], Jens Eriksson [1], Filippo Giannazzo [2] and Rositsa Yakimova [1]

[1] Department of Physics, Chemistry and Biology, Linköping University, Linköping SE-58183, Sweden; tihomir.iakimov@liu.se (T.I.); volkh@ifm.liu.se (V.K.); jenser@ifm.liu.se (J.E.); roy@ifm.liu.se (R.Y.)

[2] CNR-IMM, Strada VIII, 5 Zona Industriale, Catania 95121, Italy; filippo.giannazzo@imm.cnr.it

* Correspondence: ivan.shtepliuk@liu.se; Tel.: +46-707-6652-4089

Academic Editor: Helmut Cölfen

Received: 1 May 2017; Accepted: 31 May 2017; Published: 2 June 2017

Abstract: In spite of the great expectations for epitaxial graphene (EG) on silicon carbide (SiC) to be used as a next-generation high-performance component in high-power nano- and micro-electronics, there are still many technological challenges and fundamental problems that hinder the full potential of EG/SiC structures and that must be overcome. Among the existing problems, the quality of the graphene/SiC interface is one of the most critical factors that determines the electroactive behavior of this heterostructure. This paper reviews the relevant studies on the carrier transport through the graphene/SiC, discusses qualitatively the possibility of controllable tuning the potential barrier height at the heterointerface and analyses how the buffer layer formation affects the electronic properties of the combined EG/SiC system. The correlation between the sp^2/sp^3 hybridization ratio at the interface and the barrier height is discussed. We expect that the barrier height modulation will allow realizing a monolithic electronic platform comprising different graphene interfaces including ohmic contact, Schottky contact, gate dielectric, the electrically-active counterpart in *p-n* junctions and quantum wells.

Keywords: graphene; SiC; interface; buffer layer; barrier height; carrier transport

1. Introduction

Due to the never-ending miniaturization of electronic devices and integrated circuits, the spatial sizes of the materials become sufficiently small for new size-dependent physical limitations to effective carrier and heat transport to occur. Such constraints are governed to a large extent by the formation of an unstable transition layer at the heterointerface between two different materials. This is particularly the case of epitaxial graphene grown on silicon carbide (SiC), where complete decoupling of the graphene from the SiC surface is still a great challenge, and the interface significantly impacts many properties of graphene. Thus, a reliable control of heteroboundary quality and deep understanding of the physical nature of interface formation are imperative in order to produce device-quality graphene having the realistic chance to reach the market.

There exists evidence that up to 30% of the carbon atoms in the semiconductor-like transition carbon layer (called also the buffer layer, zero graphene layer or interfacial layer) are covalently bonded to the Si atoms (belonging to SiC) by sp^3 hybridized bonds [1–3]. It is believed that the first graphene layer fits into a $(6\sqrt{3} \times 6\sqrt{3})$ $R30^\circ$ surface reconstruction on SiC, and the $(6\sqrt{3} \times 6\sqrt{3})$ $R30^\circ$ unit cell ideally coincides with a graphene unit. However, recent research findings with more sensitive and precise techniques raise additional concerns about buffer layer formation and have revealed that the buffer layer is not commensurate with SiC surface reconstruction [4]. From the thermodynamic and chemical points of view, such features (namely, the formation of additional C-Si bonds at the graphene/SiC interface) are originating from the natural necessity to saturate the remaining Si dangling bonds (after high

temperature sublimation). In this context, many attempts at growing epitaxial graphene were dedicated to breaking up the covalent bonds between SiC and zero layer graphene and to saturating as-formed dangling bonds by guest species, so-called intercalants [5–14]. Experimental studies clearly reveal a strong effect of the buffer layer on the electronic properties of graphene; specifically, it was documented that due to the charge transfer through interfacial dangling bonds, the buffer layer is found to pin the Fermi level to ≈0.49 eV in the conduction band, making the material *n*-type [15]. As a consequence of the charge transfer from the interface states to graphene and spontaneous appearance of the interface dipole moment, the Fermi level and work function of graphene can be modulated, thereby determining its electroactive behavior [16]. Furthermore, the existence of a giant inelastic tunneling (50% of total tunneling current) caused by localized states at the interface layer of graphene/SiC was confirmed by atomically-resolved scanning tunneling microscopy and spectroscopy [17]. Another surprising fact related to the buffer layer effect was the observation of a small gap (~0.26–0.5 eV) in epitaxial graphene on SiC induced by breaking the sublattice symmetry, but the fundamental nature of this band gap opening is controversial [18,19]. New insights into the origin of the band-gap opening induced by the structural periodicity in the epitaxial graphene buffer layer have been recently reported by Nair et al [20]. Taking the aforementioned aspects into account, it is reasonable to assume that a control of the sp^2/sp^3 hybridization ratio in epitaxial graphene is a good strategy towards the atomistic-level engineering of the graphene/SiC heterointerface to tailor the electronic properties of graphene. Indeed, it was recently reported that epitaxial graphene, depending on the material quality, can play different roles when being interfaced with SiC, such as the ohmic contact [21], the Schottky contact [22], the gate electrode [21], the heterojunction counterpart [23] and/or even the quantum well component [24]. Although a great deal of attention has been paid to buffer layer effects, the physical reasons why the same material exhibits such diverse electronic features are not fully understood. There is still a point to be discussed: the correlation between buffer layer "physics" and mechanisms/possible scenarios underlying the electroactive behavior of epitaxial graphene.

Undoubtedly, for a deep understanding and correct interpretation of experimental data on the electronic properties of epitaxial graphene, one should pay proper attention to the role of the buffer layer. On the other hand, the presence of interfacial states at the heterointerface may be responsible for other physical processes and phenomena underlying the heat transport and ferromagnetism. In particular, perturbation of the ballistic heat transport caused by strong phonon scattering at the graphene/SiC interface was discussed in [25]. Thermal transport through graphene/SiC depending on the kind of SiC polytype, face polarity and atomic bond has been intensively investigated in [26–28]. These results show that the heat transfer is highly sensitive to the kind of interface between the graphene and SiC. Thus, solving the so-called thermal management problem can be achieved via controlling the geometry and the chemical nature of the interface region, i.e., the buffer layer.

As another example of the crucial role of the interfacial layer on the physical properties of graphene, Giesbers et al. [29] have reported on strong room temperature ferromagnetism (with magnetic moment of 0.9 μB per carbon hexagon projected area) and suggested that such ferromagnetic behavior may be attributed to an exchange interaction between the Coulomb-induced localized silicon dangling bonds (belonging to the buffer layer) and the localized mid-gap state. Zhou et al. [30] have also proposed some ideas towards using graphene/SiC interface-induced magnetism for spintronic applications.

The aim of this paper is to review the current status of the main experimental and theoretical studies of graphene on SiC towards understanding the physical nature of the interfacial layer formation and how this layer manifests itself in the carrier transport. In the next section, key features of the buffer layer structure will be described. We will discuss possible scenarios regarding the buffer layer-assisted interaction between graphene and SiC: we will show that the electroactive behavior of epitaxial graphene is strongly dependent on the interface chemistry and quality of the buffer layer. Finally, we make some concluding remarks regarding the relation between the quality of the graphene-SiC heteroboundary and the expected behavior of epitaxial graphene on SiC.

2. Electrical Properties of the Graphene/SiC Interface

Being combined in a single system, graphene and silicon carbide exhibit unique behavior under the influence of an external electric field, which differs from the behavior of the contact between the metal and the semiconductor under classical considerations. In the first place, the difference in the properties is caused by a possibility to control the work function of graphene and the polarizability of its π orbitals [31,32]. Therefore, the energy properties of the heterojunction may be purposefully altered by changing the interfacial chemistry between the materials.

Since the presence of the buffer layer significantly influences the electrical properties of the graphene/SiC structure, first of all, it is important to understand how current flows through a buffer-free graphene/SiC structure. From the theoretical point of view, there are, at least, three cases when we can avoid the formation of the buffer layer:

(1) The vertical structure for electrical measurements can be prepared by simple mechanical contact between exfoliated graphene and the desired SiC substrate. The starting point of the sample preparation in this case is a mechanical exfoliation of highly-oriented pyrolytic graphite (HOPG) by sticky tape, followed by the application of the exfoliated graphene films onto the SiC surface. From the literature analysis, we know that there are many techniques for the exfoliation of graphite based on common mechanical mechanisms [33].

(2) Graphene formed on the carbon-face SiC by high-temperature thermal decomposition of the SiC substrate can be also chosen as a sample for electrical characterization. Indeed, it has been repeatedly shown that the growth of graphene on the carbon-face SiC substrate does not promote the formation of the buffer layer [34].

(3) Another way to avoid the undesirable buffer layer is intercalation of graphene grown on the Si-face SiC substrate by high-temperature Si sublimation. The main scenario for this is to break the covalent bonds between the buffer layer and Si atoms on the SiC surface and to saturate the silicon dangling bonds. Then, the buffer layer can be converted into a new graphene layer with graphene symmetry and typical electronic structure. As was confirmed by experimental studies, H [9,35], Na [36], O [37,38], Li [39], Si [40], Au [12], F [11] and Ge [41] intercalation can transform the buffer layer into a graphene layer with enhanced electrical performance in comparison with untreated monolayer graphene, which exists on the buffer layer. Intercalant species can penetrate into the interface between the buffer layer and the Si-face SiC substrate and create the chemical bonds with topmost Si atoms, thereby causing the transformation of the buffer layer to quasi-free-standing graphene. It is interesting to note that non-metallic (for example, fluorine, oxygen and hydrogen) intercalations are expected to be more effective since they can strongly covalently interact with Si species of the SiC.

Let us consider a physical model of the contact between exfoliated graphene and uniformly-doped *n*-type silicon carbide, assuming the absence of any intermediate phases or surface states between them. In such an ideal case, the Fermi level is located at the Dirac point of graphene. Since the electron affinity of 4H-SiC (3.7 eV) is less than the work function of graphene (4.2 eV), the flow of electrons from the semiconductor exceeds the flow of electrons from the graphene (Figure 1). As a result, graphene acquires a negative charge, whereas the silicon carbide acquires a positive charge. Consequently, the built-in electric field between the contacting materials will prevent the further charge transfer from the silicon carbide to graphene. The exchange of charges between the semiconductor and graphene will proceed until the Fermi energies of the two materials and thermionic emission currents reach thermal equilibrium. As a result, near the surface of the semiconductor, energy bands are bent upward, and the contact resistance increases significantly. Chen et al. [42] reported a direct experimental observation of the band bending at the interface between epitaxial graphene and 6H-SiC by using in situ synchrotron-based photoemission spectroscopy. It was revealed that the band bending depends strongly on the polarity of the surface of the underlying substrate (Figure 2) and increases from 0.4 eV (for graphene on Si-terminated 6H-SiC) to 1.3 eV (in the case of graphene on C-terminated

6H-SiC). Obviously, this difference is caused by the unique nature of the growth kinetics and structural features of epitaxial graphene on silicon carbide substrates with different polarity faces. It is generally accepted that in the case of graphenization on a C-terminated 6H-SiC, the buffer layer is absent, and the interaction between the substrate and the graphene is largely unabated. It suggests that this graphene possesses a single linearly-dispersing π-band with the Dirac point located close to the Fermi level. However, according to some experimental data, the energy of the Dirac point may vary from +33 meV (*p*-doped) to −14 meV (*n*-doped) and even more [43]. Additional small doping may be caused by the presence of dangling bonds at the interface. Obviously, it could also affect the barrier height and electron transport through the interface. As has been shown in the work of Jayasekera and others [44], in the case of an unpassivated interface, the main source of electron doping is dangling bonds on the remaining carbon atoms (Figure 3a), while the energy states associated with dangling bonds on the silicon atoms are located in the valence band 1 eV above the Fermi level, and their effect can be neglected. A partial passivation of the dangling bonds on the carbon atoms (dangling bonds on silicon atoms still remain) leads to the strong interaction of silicon species with graphene (Figure 3b), and thus, graphene becomes like a buffer layer, similarly to the case of the graphenization of the Si-face SiC substrate. At the same time, the total surface passivation leads to the fact that interaction between the graphene surface and silicon carbide is weakened so that the completely detached carbon layer acquires the properties of a neutral graphene (Figure 3c).

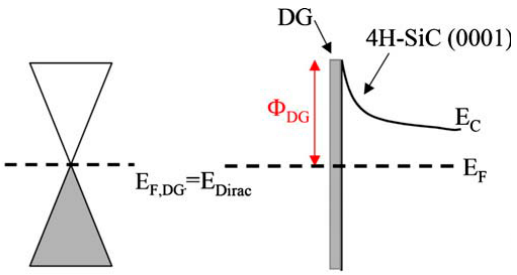

Figure 1. Energy band diagram of the graphene Schottky contact to silicon carbide (4H-SiC) [9]. To exclude the buffer layer effect on Schottky barrier formation, the authors used the graphene exfoliated from highly oriented pyrolytic graphite and deposited on 4H-SiC. DG denotes the deposited graphene on the SiC substrate, without the buffer layer [15]. E_C represents the energy of the conduction band edge; E_F is the Fermi energy for the bulk 4H-SiC; $E_{F,DG}$ is the Fermi energy of exfoliated graphene, which was directly deposited on the SiC surface. Φ_{DG} is the Schottky barrier height. E_{Dirac} corresponds to the Dirac point energy. Due to the absence of the buffer layer (only weak van der Waals-like interaction between DG and the Si substrate occurs), $E_{F,gr}$ corresponds to the Dirac point energy. Reprinted from Sonde et al. [15]. Copyright (2009) with permission from The American Physical Society.

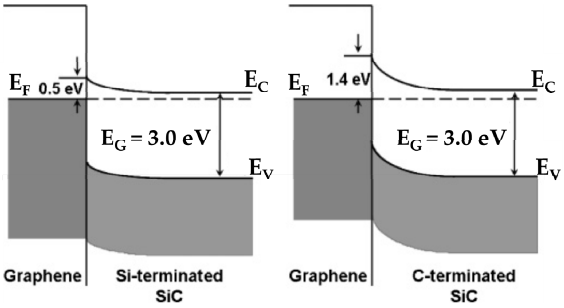

Figure 2. Band line-up at the interfaces between epitaxial graphene and (left panel) the Si-terminated 6H-SiC (0001) and (right panel) the C-terminated 6H-SiC [42]. E_C and E_V represent the energies of the conduction and valence band edge, respectively. E_F is the Fermi energy. The Fermi levels of the two materials are aligned. E_G is the band gap energy of the 6H-SiC. Reprinted from Chen et al. [42]. Copyright (2010) with permission from The Japan Society of Applied Physics.

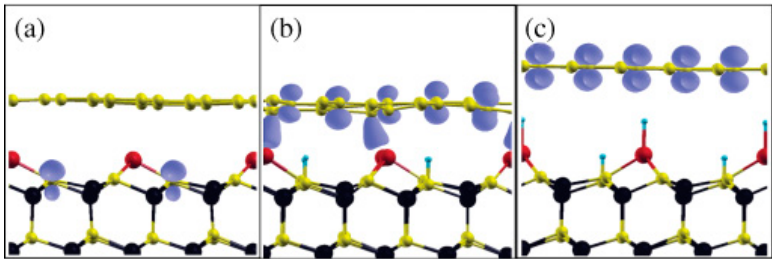

Figure 3. Possible configurations of the graphene/SiC(0001) interface and corresponding localized density of states (at the Dirac point): (**a**) unpassivated, (**b**) half-passivated and (**c**) fully-passivated systems [44]. Red atoms correspond to silicon adatoms; black atoms represent silicon atoms belonging to SiC bulk; yellow balls are C atoms; and cyan atoms are H species. Electron density isosurfaces (blue color) correspond to 0.15×10^{-3} electrons. Reprinted from Jayasekera et al. [44]. Copyright (2011) with permission from The American Physical Society.

In the third case of the absence of a buffer layer, after exposure to intercalants, we consider how hydrogen intercalation effects the electrical properties of the vertical graphene/SiC structure. As has been reported by Dharmaraj et al. [45], the vertical structure composed of as-grown epitaxial graphene and the Si-face SiC substrate exhibits a rectifying behavior with large leakage current under reverse bias (the Schottky barrier height in this case is approximately equal to 0.55 $\pm$ 0.05 eV). The authors ascribed this quite low value of the Schottky barrier height to the enhanced density of unsaturated silicon bonds in the vicinity of the interface. For correctness, the covalently bound C atoms should be also taken into account. Due to these reasons, Fermi level pinning induced by charge transfer occurs. The band diagram presented in Figure 4a clearly demonstrates that both the presence of silicon dangling bonds and the buffer layer leads to strong *n*-type doping of graphene and, as a consequence, an increase of the work function and reduction of the Schottky barrier height. During hydrogen intercalation, hydrogen species simultaneously saturate the silicon dangling bonds and break partially the covalent bonds between the buffer layer and the Si-terminated surface of SiC, thereby decoupling the buffer layer. As a result of the removal of the buffer layer and the partial saturation of unsaturated Si bonds, the hydrogen-intercalated epitaxial graphene/SiC structure demonstrates improved rectifying behavior with low leakage current in the reverse bias regime (the Schottky barrier height after intercalation procedure was estimated to be 0.75 $\pm$ 0.05 eV). As can be seen from Figure 4b, an increase in the value of the Schottky barrier height can be explained by Fermi level depinning induced by the reduction of the density of the unsaturated Si bonds and *n*-type doping of graphene. A complete passivation of the Si-terminated surface may lead to a change in the conductivity type of graphene. The change from *n*-type to *p*-type results in the modification of the band bending from upward bending to downward bending, and thus, the electrical properties of the graphene/SiC structure can be also modified.

In the case of epitaxial graphene films on the Si-face of SiC substrates, a carbon-rich buffer layer with partial sp^3 hybridization is always formed [46]. As mentioned above, the buffer layer substantially affects the electronic properties of graphene and causes pinning of the Fermi level and the subsequent reduction of the Schottky barrier height (Figure 5). In particular, it was shown that in the absence of the buffer layer, the barrier height is 0.85 $\pm$ 0.06 eV (buffer-free deposited graphene/4H-SiC) [15] and 0.75 $\pm$ 0.05 eV (buffer-free hydrogen-intercalated graphene/4H-SiC) [45], whereas the structure comprising a buffer layer exhibits a significantly reduced barrier height of 0.36 $\pm$ 0.1 eV (epitaxial graphene/4H-SiC) [15] and 0.55 $\pm$ 0.05 eV (epitaxial graphene/4H-SiC) [45].

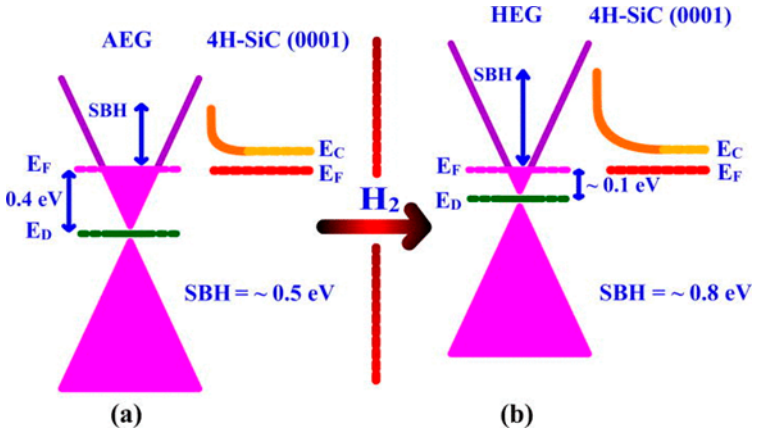

Figure 4. Energy band diagram of vertical Schottky barrier diodes: (**a**) as-deposited epitaxial graphene/4H-SiC(0001) and (**b**) hydrogen-intercalated graphene/4H-SiC(0001). AEG and HEG denote as-grown epitaxial graphene and hydrogen intercalated epitaxial graphene, respectively. During hydrogen intercalation, the Dirac point of graphene (E_D) is shifted towards E_F, thereby leading to the increase in the work function of graphene and the Schottky barrier height (SBH) [45]. Reprinted from Dharmaraj et al. [45]. Copyright (2016) with permission from The American Institute of Physics (AIP).

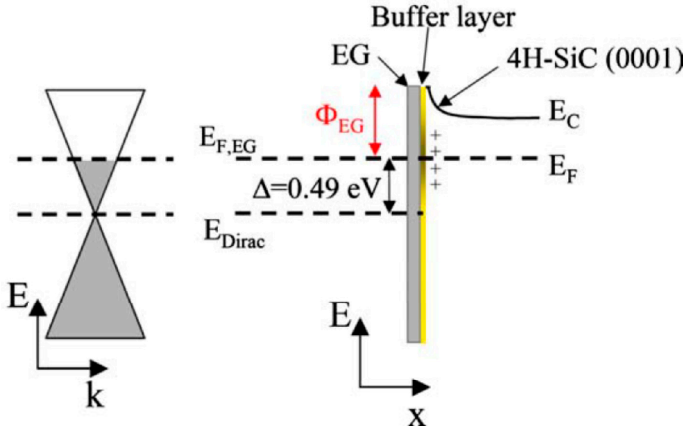

Figure 5. Band diagram of Schottky contact between graphene and SiC in the presence of a buffer layer at the interface [15]. EG denotes the epitaxial graphene on SiC substrate, with the buffer layer. E_C represents the energy of the conduction band edge; E_F is the Fermi energy for the bulk 4H-SiC; $E_{F,EG}$ is the Fermi energy of epitaxial graphene grown on the SiC surface by the thermal decomposition technique. Φ_{EG} is the Schottky barrier height. E_{Dirac} corresponds to the Dirac point energy. Due to the presence of the buffer layer, the Fermi level pinning above the Dirac point occurs. Reprinted from Sonde et al. [15]. Copyright (2009) with permission from The American Physical Society.

3. Experimental Control of the Barrier Height at the Graphene/SiC Interface

In some cases, the height and the width of the potential barrier become low/narrow enough for the electrons to easily tunnel through or overcome the barrier. In this case, the epitaxial graphene demonstrates an ohmic behavior with respect to the silicon carbide, and a linear current-voltage characteristic has been observed [21,45,47]. Apparently, it is caused by increasing the density of unsaturated dangling bonds contributing to the pinning of the Fermi level and leading to a significant doping of epitaxial graphene. In fact, increased sp^3 hybridization at the interface will result in the appearance of additional conduction channels, whereby there is a significant decrease of the contact resistance. Hertel et al. [47] have studied the electrical properties of the graphene/SiC heterointerface by a linear transfer length method. It was shown that the formation of an ohmic contact to the

weakly-doped 6H-SiC is associated with the low energy barrier Φ_B = 0.3 eV between the epitaxial graphene and 6H-SiC due to a small mismatch between the work functions of both materials. As a consequence, the electrons can overcome this barrier at ambient temperature, causing a current flow. The contact resistance can be improved by increasing the donor concentration through ion implantation under the contact. This reduces the barrier width, and tunneling through the barrier creates an additional conduction channel. In the same study, a comparative analysis of the electrical properties of two partners (graphene-4H-SiC and graphene-6H-SiC) was carried out. Since 4H-SiC has a lower value of the work function (by 0.3 eV), compared with 6H-SiC, a higher Schottky barrier of Φ_B = 0.6 eV is formed at the interface graphene/4H-SiC, thereby contributing to an increase of the contact resistance. In turn, the work function of graphene varies significantly with the number of layers (Figure 6) as was reported in a recent paper by Mammadov et al. [48]. In particular, it was found that the buffer layer has a reduced work function of 3.89 ± 0.05 eV, and every subsequent layer leads to increasing the work function, reaching a value of 4.43 ± 0.05 eV for the case of trilayer graphene. On the other hand, annealing of the zero graphene layer in an ultra-pure hydrogen environment leads to the growth of quasi-free-standing monolayer (QFMLG) graphene with a lack of buffer layer. QFMLG has a much greater work function of about 4.79 ± 0.05 eV. At that, the work function decreases with increasing numbers of layers to a value of 4.63 ± 0.05 eV for the quasi-free-standing trilayer graphene (QFTLG). From a practical point of view, this is a very important result, because the optimum performance of devices based on Schottky diodes requires a constant and uniform barrier height across the interface, not varying over the interfacial surface. Samples with a non-uniform thickness will demonstrate a wide variation of values of the work function and Schottky barrier height for the entire sample area. Indeed, as can be seen from the histogram in Figure 7, different authors reported on the large spread of this parameter for Schottky diodes based on nominally the same material [22].

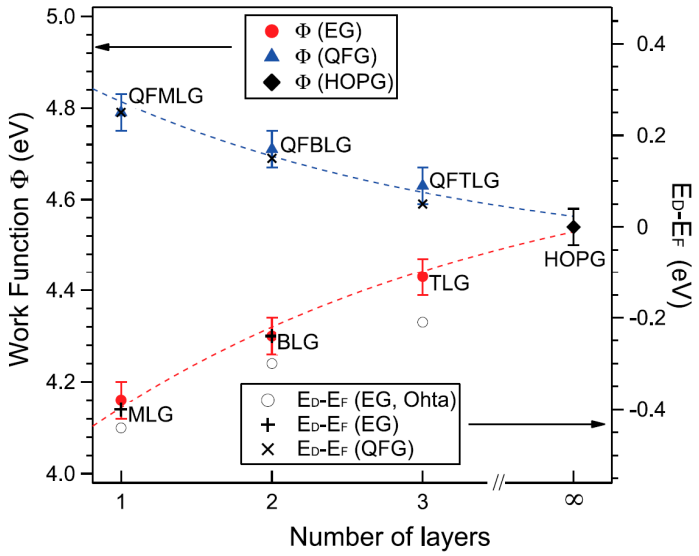

Figure 6. Dependence of the work function of epitaxial graphene (EG) with the buffer layer (red symbols) and buffer-free quasi-free-standing graphene (blue symbols) on the number of layers [48]. Abbreviation of QFG means quasi-free-standing graphene. The black symbols correspond to the position of the Dirac point with respect to the Fermi level for epitaxial graphene and quasi-free standing graphene. Reprinted from Mammadov et al. [48]. Copyright (2017) with permission from Institute of Physics Publishing Ltd. HOPG, highly-oriented pyrolytic graphite.

As can be seen from this histogram, the Schottky barrier height at the graphene/SiC heterointerface is strongly sensitive to the growth method and the graphene thickness. Furthermore, as was reported earlier, the unintentional presence of unavoidable natural ripples and ridges in epitaxial

graphene on SiC may also cause the fluctuations in the Schottky barrier height [49–54]. The key factors influencing the uniformity of the Schottky barrier height for graphene/SiC structures are the homogeneity of the graphene thickness, the quality of the grown interface (defects, pits, dislocations, surface roughness), the kind of grown interface (SiC polytypism, face polarity) and the growth conditions. We found that the Schottky junctions formed by the high-temperature Si sublimation approach [55] exhibit the smallest standard deviation of the mean value of the Schottky barrier height. This can be explained by the fact that the graphenization process via thermal decomposition of SiC promotes the formation of large-scale homogeneous epitaxial graphene layers [56–59].

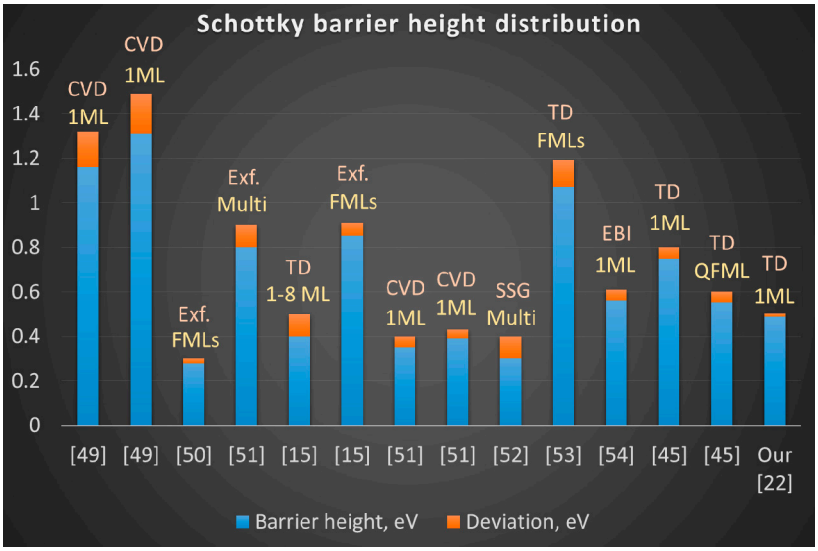

Figure 7. Histogram of the Schottky barrier height distribution for graphene on SiC made by different techniques and different thicknesses.

Indeed, our *I-V* measurements of the graphene (99% of the total coverage is monolayer)/4H-SiC(0001) vertical device revealed the very stable rectifying behavior of the graphene/SiC diode (Figure 8). In line with the statistical distribution, the determined values of the Schottky barrier height range from 0.46 to 0.503 eV for the graphene/SiC junction, while the ideality factor ranges from 1.011 to 1.026. The standard deviations yield 0.013 eV and 0.0049 for the two parameters, respectively. We determined that the mean values of Schottky barrier height and ideality factor of the Schottky diode are 0.4879 eV and 1.018, respectively. The extracted value of the Schottky barrier height coincides well with the theoretical value of 0.5 eV. In comparison to previously-reported results, our sample (by virtue of the high thickness uniformity) demonstrates the smallest reported value of the standard deviation for the Schottky barrier height.

Multifunctional properties of the graphene-silicon carbide interface have been used to create a monolithic transistor based on a single platform (Figure 9) [21]. It should be noted that in this case, the graphene plays a dual role. On the one hand, the graphene forms ohmic contacts to silicon carbide, thus acting as the source and drain. On the other hand, the graphene forms a Schottky barrier and plays the role of the gate contact. Interestingly, the presence or absence of the buffer layer is the key factor that determines the role of graphene. Epitaxial graphene monolayer (electron density and carrier mobility are equal to $n = 10^{13}$ cm^{-2}, $\mu_e = 900$ cm^2·V·s^{-1}, respectively) with a carbon-rich buffer layer underneath (Figure 9b) exhibits an ideal ohmic behavior, despite the weak doping level of silicon carbide. Upon hydrogen intercalation (in H_2 atmosphere at 850 °C), the buffer layer is decoupled from the substrate, and quasi-free-standing bilayer graphene is formed (Figure 9c) with the following parameters: hole density $p = 10^{13}$ cm^{-2}, $\mu_h = 2.000$ cm^2·V·s^{-1} at room temperature. Indeed, in this case, breaking of the covalent bonds between the graphene and silicon carbide occurs, and the remaining dangling bonds are saturated with hydrogen atoms. As a result, the buffer layer is converted to an

additional layer of graphene. Since quasi-free-standing bilayer graphene (QFBLG) on SiC exhibits rectifying behavior inherent to the Schottky diode, it can be used as the gate contact. Analysis of the capacitance-voltage and current-voltage characteristics allowed estimating both the lower limit of barrier height ($\phi_{B,IV}$ = 0.9 eV) and the upper limit ($\phi_{B,CV}$ = 1.1 eV ... 1.6 eV). The high value of the barrier height and negligible leakage current meet the main requirements of the Schottky diodes. Despite the fact that QFBLG forms a Schottky contact to *n*-type SiC, large fluctuations in the Schottky barrier height over the entire area of contact between the two materials are still a significant problem, limiting the fabrication of high-performance transistors. Importantly, a complete deactivation of the buffer layer due to the hydrogen-induced intercalation could lead to the conductivity type switching in graphene from *n*-type to *p*-type. This phenomenon is due to the intrinsic spontaneous polarization of the hexagonal silicon carbide substrate and results in both a substantial increase in the Schottky barrier height of more than >1 eV [45] and even the activation of another kind of current in a *p*-*n* junction, which is governed by recombination or generation processes within the *p*-*n* diode structure.

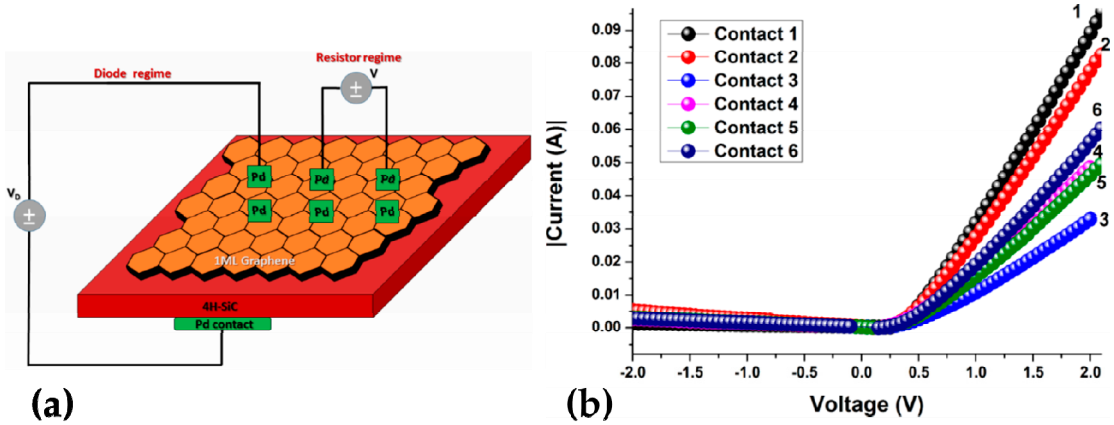

Figure 8. (**a**) Sketch of the graphene/4H-SiC vertical device and (**b**) current-voltage characteristics of the vertical graphene-4H-SiC device. The *y*-axis indicates the absolute values of current. Palladium contacts (1–6) are positioned at different places on the graphene surface [22]. Reprinted from Shtepliuk et al. [22]. Copyright (2016) Shtepliuk et al.; licensee Beilstein-Institut.

Butt et al. [60] demonstrated the important role of the buffer layer beneath graphene in the process of the photogeneration of carriers in a transistor. It is known that the strong interaction between the substrate and the buffer layer contributes to lowering the energy barrier, while the complete deactivation of the buffer layer will lead to a significant increase in the Schottky barrier. The aforementioned work confirmed that the absence of an energy barrier at the interface causes the carrier injection rate to become equal to the rate of the thermal generation of carriers and becomes dependent on the thickness and barrier height at the interface. Figure 10 shows the qualitative phenomenon of photo-induced electrostatic doping of graphene. The energy diagrams of the SiC/graphene interface along the direction perpendicular to the channel are shown for different injection rate limits in dark and light conditions with the illustrated charge density in SiC. As a result of the photogeneration of carriers in SiC in the light regime, holes drift in the direction of the source and drain contacts due to the voltage applied to the gate (V_{bg} = 20 V). In the absence of a barrier at the graphene/SiC interface, the injection rate is equal to the thermal generation rate, and therefore, holes do not accumulate at the interface. In this situation, spatial charge separation does not occur at the interface, and thus, the substrate-induced electrostatic effect in graphene is negligible, as shown in Figure 10b. In the presence of the energy barrier at the interface (the injection rate is less than the thermal generation rate), the drift of the photogenerated carriers from the substrate results in charge accumulation in the vicinity of the surface of the SiC (Figure 10c,d).

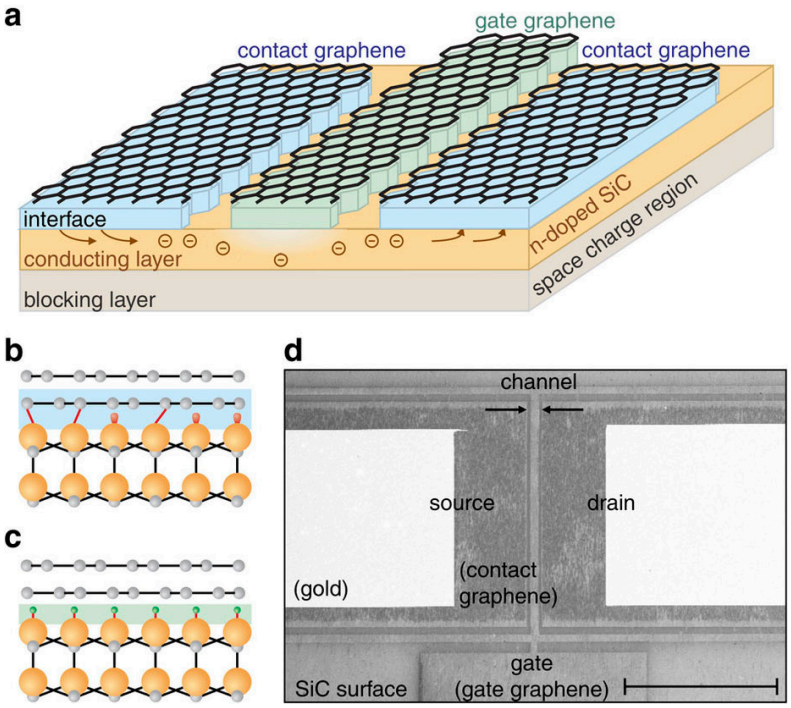

Figure 9. (**a**) Schematic of the device with two kinds of graphene: graphene as the ohmic contact for the source/drain and (**b**) and graphene as a Schottky-like gate (**c**). (**d**) An electron micrograph illustrating the realistic device configuration [21]. In (**b**,**c**), the orange atoms correspond to silicon adatoms; grey balls are C atoms; and red/green atoms are H species. Reprinted from Hertel et al. [21]. Copyright (2012) with permission from Macmillan Publishers Limited.

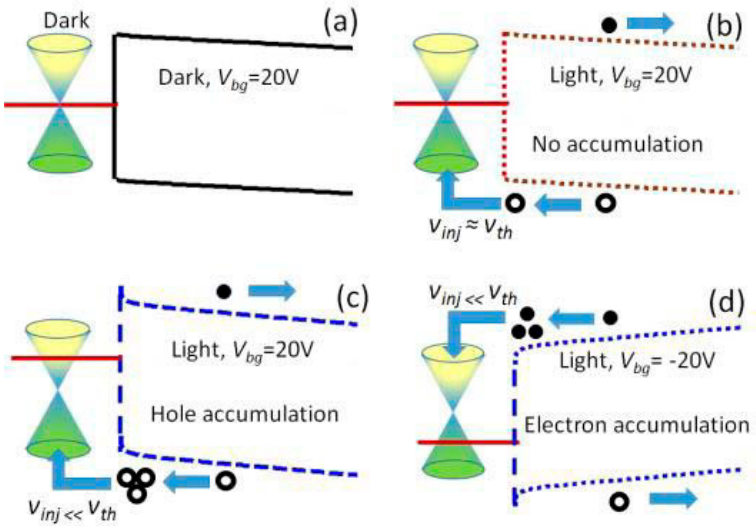

Figure 10. Band diagram of graphene/SiC interface (**a**) in dark and (**b**–**d**) under illumination. No electrostatic doping in graphene is observed in dark conditions. V_g is the voltage applied to the gate; V_{inj} is velocity of carrier injection from the SiC into the graphene; and V_{th} is the carrier's thermal velocity, respectively. Graphene becomes *n*-type after applying forward bias in the "light" regime (**c**) and *p*-type after applying a reverse bias in the light "regime" (**d**) [60]. Reprinted from Butt et al. [60]. Copyright (2015) with permission from IEEE.

At this point, we would like to draw the reader's attention to the difference between the aforementioned current transport mechanisms through the graphene/SiC heterointerface:

(1) If the potential barrier is wide and high (as in the case of stable Schottky diode, formed on the buffer-layer free graphene and SiC), the current is driven by thermal excitation of the electrons and their transfer from the silicon carbide into graphene (thermionic emission).
(2) If the potential barrier at the interface is rather narrow (due to the strong interaction between the buffer layer and the topmost layers of silicon carbide), then current flows due to tunneling through energy barriers regardless of their width and energy height (ohmic contact formation).
(3) In some intermediate cases, epitaxial graphene may consist of sp^2-bonded carbon atoms with a small fraction of sp^3 hybridized carbon species bound to SiC (less than 30%). It is clear that under such conditions, the currents through the interface are regulated by two competing mechanisms: thermal excitation of carriers and their tunneling through the top of the barrier. In this scenario, a Schottky barrier is high enough to provide rectifying behavior. On the other hand, the leakage current will be increased substantially, thus degrading the performance of the diode.

4. Observations of Uncommon Phenomena at the Graphene/SiC Interface

It is important to note that some heterostructures consisting of epitaxial graphene on silicon carbide can exhibit behavior that significantly differs from both the ohmic contact and the Schottky contact. Contrary to the Schottky diodes, the potential barrier height (2.53 eV [23], 2.70 eV [61] and 2.90 eV [24]) in such structures can be as large as the band gap energy of silicon carbide (E_g = 3.23 eV). There are possible explanations for these phenomena, which are connected with specific features of the graphenization of SiC, unusual polarization-induced *p*-type doping of the epitaxial graphene or even more likely the formation of the *p*-*n* junction between graphene and SiC.

Indeed, Andersson et al. [23] found that the *I*-*V* characteristics across the *n*-type epitaxial graphene/*p*-SiC interface are better described by a *p*-*n* diode model than by thermionic emission. According to this theory, the carrier transport mechanism through the anisotype graphene/silicon carbide *p*-*n* junction is governed by diffusion and recombination of carriers in the quasi-neutral region. In order to confirm the applicability of the theory, electroluminescence studies were performed, allowing one to obtain a direct proof of the radiative recombination in the silicon carbide layers. If a forward or reverse-biasing voltage is applied across the *p*-*n* junction, a visible emission at the edges of the graphene mesa is observed, as shown in the in Figure 11b. The observed peak at 410 nm (3.02 eV) is associated with an optical radiative transition between the acceptor level and the conduction band in SiC. This proves the injection of minority carriers in silicon carbide from the graphene side. In principle, the injection of minority carriers is also possible in the case of a Schottky diode, but the injection ratio is negligible because of the low carrier density in the SiC [62]. Therefore, these experimental observations are more likely associated with the formation of a heterojunction than a Schottky barrier. It is assumed that in this case, an anisotype (*p*-*n*) transition type 1 is formed, with a dominant current due to recombination and diffusion in the forward bias regime and reverse bias leakage caused by thermal generation. The band diagram of the system being studied is shown in the Figure 11a.

In another work, Anderson et al. [61] have performed a comparative analysis of the electrical properties of the anisotype *p*-*n* junction (*n*-type epitaxial graphene/*p*-type SiC) and isotype *p*-*p* junction (*p*-type epitaxial graphene/*p*-type SiC) in the dark and light regimes. Band diagrams for these devices are shown in Figure 12.

Expectedly, the *p*-*n* junction exhibits well-pronounced rectifying behavior with small leakage current (Figure 13a), suggesting the dominating character of the drift-diffusion mechanism of current transport. Within this model, the leakage current at the reverse bias is negligible, because it consists of only diffusion and thermal generation current components. On the other hand, the *p*-type graphene/*p*-type SiC structure behaves like the typical isotype *p*-*p* junction or the Schottky diode (Figure 13b). The charge transport through the device with the dominant role of the majority carriers in the forward bias regime is governed by thermionic emission, whereas the leakage current in the reverse bias mode increases linearly with increasing reverse voltage.

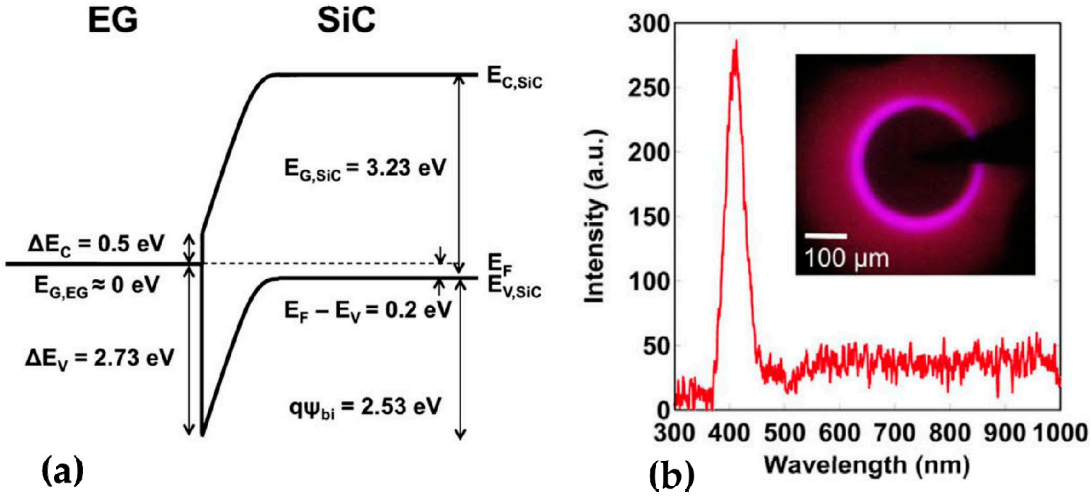

Figure 11. (**a**) Energy diagram of the EG/*p*-SiC structure; (**b**) Electroluminescence (EL) spectrum and EL image collected from EG/*p*-SiC at high forward bias [23]. $E_{G,SiC}$ is the band gap energy of the bulk SiC; $E_{G,EG}$ is the band gap energy of the epitaxial graphene. E_F is the Fermi energy; E_C (E_V) is the energy of the conduction (valence) band edge; and $q\psi_{bi}$ is the barrier height, respectively. ΔE_V and ΔE_C are the expected valence and conduction band discontinuities. Reprinted from Anderson et al. [23]. Copyright (2012) with permission from IEEE.

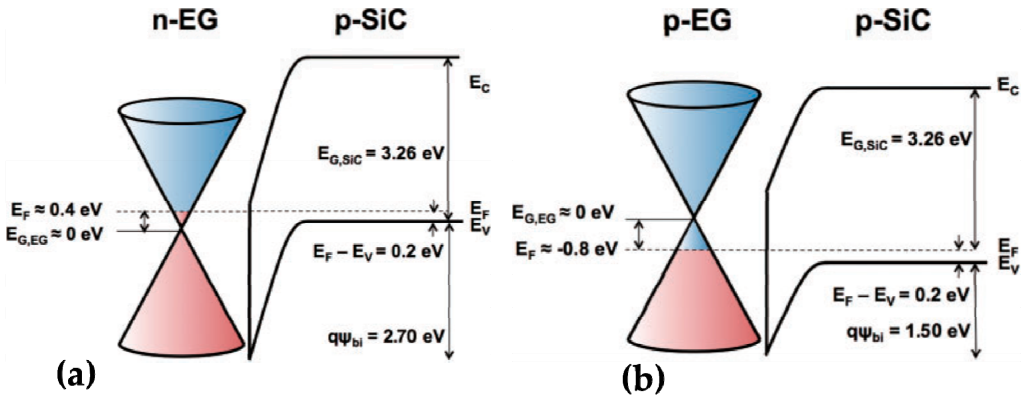

Figure 12. Schemes showing the band diagrams for the *n*-type epitaxial graphene/*p*-type SiC (**a**) and *p*-type epitaxial graphene/*p*-type SiC (**b**) junctions [61]. $E_{G,SiC}$ is the band gap energy of the bulk SiC; $E_{G,EG}$ is the band gap energy of the epitaxial graphene. E_F is the Fermi energy; E_C (E_V) is the energy of the conduction (valence) band edge; and $q\psi_{bi}$ is the barrier height, respectively. Reprinted from Anderson et al. [61]. Copyright (2015) with permission from The Japan Society of Applied Physics.

Interestingly, some authors reported that bound quantum states may occur at the graphene/*n*-type SiC heterointerface [24]. This phenomenon is probably due to the formation of deep (2.9 eV) and narrow (2.15 Å) barriers, the so-called layered nanostructure with the hole quantum well (QW) potential relief (Figure 14a illustrates the band diagram of the investigated structure). The authors emphasized that the carbon-rich buffer layer with surface reconstruction $(6\sqrt{3} \times 6\sqrt{3})$ $R30°$ plays the role of the wide band-gap layer, since the chemical interaction between the interfacial layer and SiC diminishes the π-electronic subsystem and opens a gap. According to the literature data, such an energy gap can reach ~2 eV for the $(6\sqrt{3} \times 6\sqrt{3})$ $R30°$ layer [63]. Due to these features, the top of the graphene valence band (shaded area in Figure 14a) looks like a hole quantum well, and the quantum confinement of the electrons normal to graphene plane is expected. As can been seen from Figure 14b, three distinguished peaks near the Fermi level at energies of E_1 = 0.3 eV, E_2 = 1.2 eV and E_3 = 2.6 eV are present on the

valence band density of states. These singularities were attributed to the quantum well bound states. Taking into account the fact that these peaks are absent on the valence band spectra of graphite and SiC substrate, they have a graphene-like nature. In addition, the authors reasonably assumed that the observed valence band features (E_1, E_2 and E_3) cannot be assigned to the buffer layer because previous studies showed that the ($6\sqrt{3} \times 6\sqrt{3}$) R30° buffer layer is only responsible for the appearance of two additional peaks g_1 and g_2 at binding energies of 0.5 and 1.6 eV [1,64], which do not coincide with the E_1, E_2 and E_3 peaks.

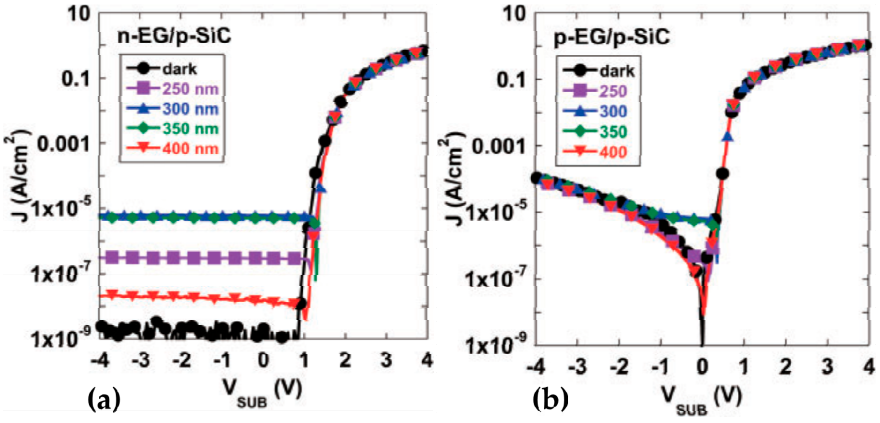

Figure 13. Dependences of the current-voltage characteristics on the illumination wavelength for different devices: *n*-type epitaxial graphene/*p*-type SiC (**a**) and *p*-type epitaxial graphene/*p*-type SiC (**b**) junctions [61]. Reprinted from Anderson et al. [61]. Copyright (2015) with permission from The Japan Society of Applied Physics.

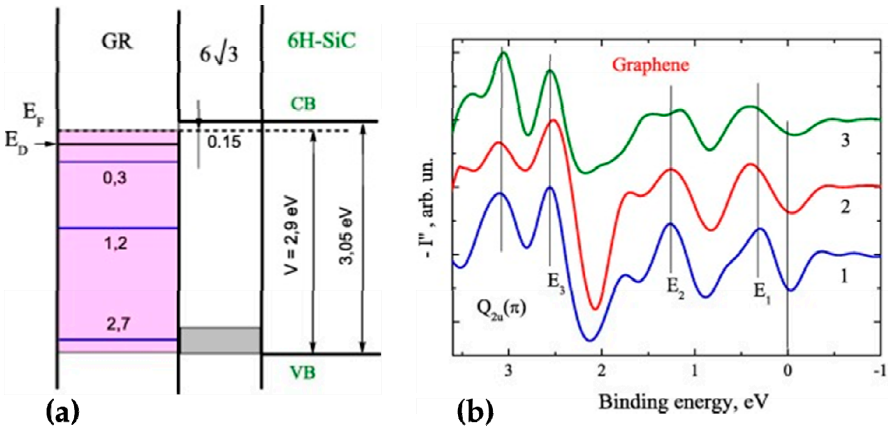

Figure 14. (**a**) Energetic diagram of the hole quantum well formed by graphene on SiC with the carbon-rich buffer layer; (**b**) Inverse second derivatives of the valence band photoemission spectra of epitaxial graphene collected from different sample areas (1–3) [24]. E_D is the Dirac point energy; E_F is the Fermi energy; CB is the bottom of the conduction band; and VB is the top of the valence band, receptively. Reprinted from Mikoushkin et al. [24]. Copyright (2015) with permission from Elsevier.

Table 1 summarizes potential barrier heights for different vertical structures composed of graphene and SiC substrates by different methods.

Table 1. Barrier heights for current transport through vertical graphene/SiC structures depending on the preparation technique. ML: the monolayer; CVD: chemical vapour deposition; HOPG: highly-oriented pyrolytic graphite.

Junction	Growth Method	Thickness	Barrier Height, eV	Reference
Gr/*n*-4H-SiC	Si sublimation	1–8 ML	0.36 ± 0.1	[15]
Gr/*n*-4H-SiC	Exfoliation	Few ML	0.85 ± 0.06	[15]
Gr/n-Si-6H-SiC	Thermal decomposition	2 ML	0.9	[21]
Gr/*n*-Si-4H-SiC	Si sublimation	1 ML	0.487 ± 0.013	[22]
Gr/*p*-4H-SiC	Si sublimation	1 ML	2.53	[23]
Gr/*n*-Si-6H-SiC	Si sublimation	1.6 ML	2.90	[24]
p-Gr/*p*-4H-SiC	Si sublimation	3 ML	1.5	[45]
Gr/n-Si-4H-SiC	Low energy e-beam irradiation	1 ML	0.556 ± 0.05	[45]
Gr/*n*-Si-4H-SiC	CVD	1 ML	1.16 ± 0.16	[49]
Gr/*n*-C-4H-SiC	CVD	1 ML	1.306 ± 0.18	[49]
Gr/*n*-SiC	Exfoliation	Few ML	0.28 ± 0.02	[50]
Gr/n-Si-6H-SiC	CVD	1 ML	0.35 ± 0.05	[51]
Gr/*n*-C-4H-SiC	CVD	1 ML	0.39 ± 0.04	[51]
Graphite/*p*-4H-SiC	Solid state graphitization	Multilayer	2.7 ± 0.1	[52]
Graphite/n-4H-SiC	Solid state graphitization	Multilayer	0.3 ± 0.1	[52]
Gr/*n*-Si-4H-SiC	Thermal decomposition	Few ML	1.066 ± 0.12	[53]
Gr/*n*-4H-SiC	Exfoliation of HOPG	Multilayer	0.8 ± 0.1	[54]
n-Gr/*p*-4H-SiC	Si sublimation	3 ML	2.7	[61]
Gr/*n*-4H-SiC	Si sublimation	Few ML	0.08	[65]
Gr/n-Si-4H-SiC	Electron-beam irradiation	2 ML	0.58	[66]
Gr/*n*-4H-SiC	CVD	1 ML	0.91	[67]
Gr/*n*-Si-6H-SiC	Thermal decomposition	2 ML	1.15–1.45	[68]
HOPG/*n*-SiC	Van der Waals adherence of cleaved HOPG	Multilayer	1.15	[69]

From our previous work [70], we know that the quality of graphene (thickness, uniformity) and its physical properties are highly sensitive to the status of the SiC substrate, including the miscut angle, kind of polytype and face polarity. Therefore, the reliable control of the barrier height requires a clear understanding of the fundamental relation between the properties of the SiC substrate and the quality of the graphene layers.

5. Concluding Remarks

The electrical properties of the graphene/silicon carbide heterointerface have been discussed in order to illustrate the buffer layer role in carrier transport via the heterointerface and the fundamental reasons underlying the barrier height modulation. Although the theoretical value of the barrier height was estimated to be 0.5 eV, it could not be achieved in most experiments, and large deviations from the ideal value, as well as barrier height inhomogeneity have been frequently observed. Such behavior can be understood in terms of structural imperfections (high sp^2/sp^3 hybridization ratio, thickness nonuniformity, domains with different doping levels, ripples, etc.) unintentionally appearing during the graphenization process. In this regard, a reliable and precise control of the barrier height is imperative for further implementation of the epitaxial graphene technology into realistic Schottky diode-based electronic devices. Possible ways to achieve such control might involve the complete decoupling of the carbon-rich buffer layer from the substrate. Indeed, the buffer layer-free samples always offer an enhanced value of the barrier height and a more pronounced Schottky-type rectifying behavior with current transport governed by the thermionic emission mechanism. In the case of the strong interaction between the buffer layer and SiC, deviations from theoretical predictions are observed towards reduced barrier heights. Furthermore, fine tuning of the interfacial chemistry (mainly the sp^2/sp^3 hybridization ratio) makes possible the transition from the Schottky-like contact to the ohmic-like one. An analysis of the literature data led us to deduce that the rarely observed high potential barrier (>2 eV) at the interface seems to be a key factor, which primarily determines the

dominant role of the drift-diffusion mechanism in charge transport via the heterostructure. We believe that the barrier height modulation is a good strategy for the development of a monolithic electronic platform comprising the different kinds of graphene behaviors (ohmic contact, Schottky contact, gate dielectric, electrically-active counterpart in *p-n* junction and quantum well) by the most promising and controllable graphitization technique: high-temperature thermal decomposition of the SiC substrate in an argon ambient environment.

Future work should aim at deeper investigations of the relationship "carrier density in graphene-thickness of graphene-barrier height at the interface" to provide more complete physical insights into the current transport via the graphene/SiC interface and facilitate further applications.

Acknowledgments: The project has received funding from the European Union's Horizon 2020 research and innovation program under Grant Agreement No. 696656. The authors would like to thank the financial support via the Vetenskapsrådet (VR) grant 621-2014-5805 and Stiftelsen för strategisk forskning (SSF GMT14-0077, SSF RMA15-0024). Ivan Shtepliuk acknowledges the support from Wallenberg foundation and Ångpanneföreningens Forskningsstiftelse (Grant 16-541). Volodymyr Khranovskyy acknowledges the Swedish Research Council (VR) Marie Skłodowska Curie International Career Grant #2015-00679 "GREEN 2D FOX" and ÅForsk (Grant 14-517).

Author Contributions: Ivan Shtepliuk, Jens Eriksson, Filippo Giannazzo and Rositza Yakimova conceived of the idea and co-wrote the paper. Volodymyr Khranovskyy and Tihomir Iakimov commented on and improved the manuscript. All authors discussed the results.

Conflicts of Interest: The authors declare no competing financial interests.

References

1. Emtsev, K.V.; Speck, F.; Seyller, T.; Ley, L.; Riley, J.D. Interaction, growth, and ordering of epitaxial graphene on SiC(0001) surfaces: A comparative photoelectron spectroscopy study. *Phys. Rev. B* **2008**, *77*, 155303. [CrossRef]
2. Emery, J.D.; Detlefs, B.; Karmel, H.J.; Nyakiti, L.O.; Gaskill, D.K.; Hersam, M.C. Chemically Resolved Interface Structure of Epitaxial Graphene on SiC(0001). *Phys. Rev. Lett.* **2013**, *111*, 215501. [CrossRef] [PubMed]
3. Strupinski, W.; Grodecki, K.; Caban, P.; Ciepielewski, P.; Jozwik-Biala, I.; Baranowski, J.M. Formation mechanism of graphene buffer layer on SiC(0001). *Carbon* **2015**, *81*, 63. [CrossRef]
4. Conrad, M.; Wang, F.; Nevius, M.; Jinkins, K.; Celis, A.; Nair, M.N.; Taleb-Ibrahimi, A.; Tejeda, A.; Garreau, Y.; Vlad, A.; et al. Wide Band Gap Semiconductor from a Hidden 2D Incommensurate Graphene Phase. *Nano Lett.* **2017**, *17*, 341. [CrossRef] [PubMed]
5. Stöhr, A.; Forti, S.; Link, S.; Zakharov, A.A.; Kern, K.; Starke, U.; Benia, H.M. Intercalation of graphene on SiC(0001) via ion implantation. *Phys. Rev. B* **2016**, *94*, 085431. [CrossRef]
6. Visikovskiy, A.; Kimoto, S.; Kajiwara, T.; Yoshimura, M.; Iimori, T.; Komori, F.; Tanaka, S. Graphene/SiC(0001) interface structures induced by Si intercalation and their influence on electronic properties of graphene. *Phys. Rev. B* **2016**, *94*, 245421. [CrossRef]
7. Caffrey, N.M.; Johansson, L.I.; Xia, C.; Armiento, R.; Abrikosov, I.A.; Jacobi, C. Structural and electronic properties of Li-intercalated graphene on SiC(0001). *Phys. Rev. B* **2016**, *93*, 195421. [CrossRef]
8. Caffrey, N.M.; Armiento, R.; Yakimova, R.; Abrikosov, I.A. Charge neutrality in epitaxial graphene on 6H-SiC(0001) via nitrogen intercalation. *Phys. Rev. B* **2015**, *92*, 081409. [CrossRef]
9. Riedl, C.; Coletti, C.; Iwasaki, T.; Zakharov, A.A.; Starke, U. Quasi-Free-Standing Epitaxial Graphene on SiC Obtained by Hydrogen Intercalation. *Phys. Rev. Lett.* **2009**, *103*, 246804. [CrossRef] [PubMed]
10. Sandin, A.; Jayasekera, T.; Rowe, J.E.; Kim, K.W.; Nardelli, M.B.; Dougherty, D.B. Multiple coexisting intercalation structures of sodium in epitaxial graphene-SiC interfaces. *Phys. Rev. B* **2012**, *85*, 125410. [CrossRef]
11. Walter, A.; Jeon, K.-J.; Bostwick, A.; Speck, F.; Ostler, M.; Seyller, T.; Moreschini, L.; Kim, Y.S.; Chang, Y.J.; Horn, K.; et al. Highly *p*-doped epitaxial graphene obtained by fluorine intercalation. *Appl. Phys. Lett.* **2011**, *98*, 184102. [CrossRef]
12. Gierz, I.; Suzuki, T.; Weitz, R.T.; Lee, D.S.; Krauss, B.; Riedl, C.; Starke, U.; Höchst, H.; Smet, J.H.; Ast, C.R.; et al. Electronic decoupling of an epitaxial graphene monolayer by gold intercalation. *Phys. Rev. B* **2010**, *81*, 235408. [CrossRef]

13. Hsu, C.-H.; Ozolins, V.; Chuang, F.-C. First-principles study of Bi and Sb intercalated graphene on SiC(0001) substrate. *Surf. Sci.* **2013**, *616*, 149–154. [CrossRef]
14. Huang, L.; Xu, W.-Y.; Que, Y.-D.; Mao, J.-H.; Meng, L.; Pan, L.-D.; Li, G.; Wang, Y.-L.; Du, S.-X.; Liu, C.; et al. Intercalation of metals and silicon at the interface of epitaxial graphene and its substrates. *Chin. Phys. B* **2013**, *22*, 096803. [CrossRef]
15. Sonde, S.; Giannazzo, F.; Raineri, V.; Yakimova, R.; Huntzinger, J.-R.; Tiberj, A.; Camassel, J. Electrical properties of the graphene/4H-SiC(0001) interface probed by scanning current spectroscopy. *Phys. Rev. B* **2009**, *80*, 241406. [CrossRef]
16. Renault, O.; Pascon, A.M.; Rotella, H.; Kaja, K.; Mathieu, C.; Rault, J.E.; Blaise, P.; Poiroux, T.; Barrett, N.; Fonseca, L.R.C. Charge spill-out and work function of few-layer graphene on SiC(0001). *J. Phys. D Appl. Phys.* **2014**, *47*, 295303. [CrossRef]
17. Červenka, J.; van de Ruit, K.; Flipse, C.F.J. Giant inelastic tunneling in epitaxial graphene mediated by localized states. *Phys. Rev. B* **2010**, *81*, 205403. [CrossRef]
18. Rotenberg, E.; Bostwick, A.; Ohta, T.; McChesney, J.L.; Seyller, T.; Horn, K. Origin of the energy bandgap in epitaxial graphene. *Nature Mater.* **2008**, *7*, 258. [CrossRef] [PubMed]
19. Nevius, M.S.; Conrad, M.; Wang, F.; Celis, A.; Nair, M.N.; Taleb-Ibrahimi, A.; Tejeda, A.; Conrad, E.H. Semiconducting Graphene from Highly Ordered Substrate Interactions. *Phys. Rev. B* **2015**, *115*, 136802. [CrossRef] [PubMed]
20. Nair, M.N.; Palacio, I.; Celis, A.; Zobelli, A.; Gloter, A.; Kubsky, S.; Turmaud, J.-P.; Conrad, M.; Berger, C.; de Heer, W.; et al. Band Gap Opening Induced by the Structural Periodicity in Epitaxial Graphene Buffer Layer. *Nano Lett.* **2017**, *17*, 2681–2689. [CrossRef] [PubMed]
21. Hertel, S.; Waldmann, D.; Jobst, J.; Albert, A.; Albrecht, M.; Reshanov, S.; Schöner, A.; Krieger, M.; Weber, H.B. Tailoring the graphene/silicon carbide interface for monolithic wafer-scale electronics. *Nat. Commun.* **2012**, *3*, 957. [CrossRef] [PubMed]
22. Shtepliuk, I.; Eriksson, J.; Khranovskyy, V.; Iakimov, T.; Lloyd Spetz, A.; Yakimova, R. Monolayer graphene/SiC Schottky barrier diodes with improved barrier height uniformity as a sensing platform for the detection of heavy metals. *Beilstein. J. Nanotechnol.* **2016**, *7*, 1800. [CrossRef] [PubMed]
23. Anderson, T.J.; Hobart, K.D.; Nyakiti, L.O.; Wheeler, V.D.; Myers-Ward, R.L.; Caldwell, J.D.; Bezares, F.J.; Jernigan, G.G.; Tadjer, M.J.; Imhoff, E.A.; et al. Investigation of the Epitaxial Graphene/p-SiC Heterojunction. *IEEE Electron. Device Lett.* **2012**, *33*, 1610. [CrossRef]
24. Mikoushkin, V.M.; Shnitov, V.V.; Lebedev, A.A.; Lebedev, S.P.; Nikonov, S.Y.; Vilkov, O.Y.; Iakimov, T.; Yakimova, R. Size confinement effect in graphene grown on 6H-SiC(0001) substrate. *Carbon* **2015**, *86*, 139. [CrossRef]
25. Xu, Z.; Buehler, M.J. Heat dissipation at a graphene—Substrate interface. *J. Phys. Condens. Matter* **2012**, *24*, 475305. [CrossRef] [PubMed]
26. Hu, M.; Poulikakos, D. Graphene mediated thermal resistance reduction at strongly coupled interfaces. *Int. J. Heat Mass Transfer.* **2013**, *62*, 205. [CrossRef]
27. Li, M.; Zhang, J.; Hu, X.; Yue, Y. Thermal transport across graphene/SiC interface: Effects of atomic bond and crystallinity of substrate. *Appl. Phys. A* **2015**, *119*, 415. [CrossRef]
28. Wang, Z.; Bi, K.; Guan, H.; Wang, J. Thermal Transport between Graphene Sheets and SiC Substrate by Molecular-Dynamical Calculation. *J. Mater.* **2014**, 479808. [CrossRef]
29. Giesbers, A.J.M.; Uhlířová, K.; Konečný, M.; Peters, E.C.; Burghard, M.; Aarts, J.C.; Flipse, F.J. Interface-Induced Room-Temperature Ferromagnetism in Hydrogenated Epitaxial Graphene. *Phys. Rev. Lett.* **2013**, *111*, 166101. [CrossRef] [PubMed]
30. Zhou, P.; He, D. Modulating doping and interface magnetism of epitaxial graphene on SiC(0001). *Chin. Phys. B* **2016**, *25*, 017302. [CrossRef]
31. Yu, Y.J.; Zhao, Y.; Ryu, S.; Brus, L.E.; Kim, K.S.; Kim, P. Tuning the Graphene Work Function by Electric Field Effect. *Nano Lett.* **2009**, *9*, 3430. [CrossRef] [PubMed]
32. Castro Neto, A.H.; Guinea, F.; Peres, N.M.R.; Novoselov, K.S.; Geim, A.K. The electronic properties of graphene. *Rev. Mod. Phys.* **2009**, *81*, 109–162. [CrossRef]
33. Yi, M.; Shen, Z. A review on mechanical exfoliation for the scalable production of graphene. *J. Mater. Chem. A* **2015**, *3*, 11700–11715. [CrossRef]

34. Hass, J.; Varchon, F.; Millán-Otoya, J.E.; Sprinkle, M.; Sharma, N.; de Heer, W.A.; Berger, C.; First, P.N.; Magaud, L.; Conrad, E.H. Why Multilayer Graphene on 4H'SiC(0001) Behaves Like a Single Sheet of Graphene. *Phys. Rev. Lett.* **2008**, *100*, 125504. [CrossRef] [PubMed]
35. Virojanadara, C.; Zakharov, A.A.; Yakimova, R.; Johansson, L.I. Buffer layer free large area bi-layer graphene on SiC(0001). *Surf. Sci.* **2010**, *604*, L4–L7. [CrossRef]
36. Xia, C.; Watcharinyanon, S.; Zakharov, A.A.; Johansson, L.I.; Yakimova, R.; Virojanadara, C. Detailed studies of Na intercalation on furnace-grown graphene on 6H-SiC(0001). *Surf. Sci.* **2013**, *613*, 88–94. [CrossRef]
37. Kowalski, G.; Tokarczyk, M.; Dąbrowski, P.; Ciepielewski, P.; Możdżonek, M.; Strupiński, W.; Baranowski, J.M. New X-ray insight into oxygen intercalation in epitaxial graphene grown on 4H-SiC(0001). *J. Appl. Phys.* **2015**, *117*, 105301. [CrossRef]
38. Oliveira, M.H., Jr.; Schumann, T.; Fromm, F.; Koch, R.; Ostler, M.; Ramsteiner, M.; Seyller, T.; Lopes, J.M.J.; Riechert, H. Formation of high-quality quasi-free-standing bilayer graphene on SiC(0001) by oxygen intercalation upon annealing in air. *Carbon* **2013**, *52*, 83–89. [CrossRef]
39. Virojanadara, C.; Watcharinyanon, S.; Zakharov, A.A.; Johansson, L.J. Epitaxial graphene on 6H-SiC and Li intercalation. *Phys. Rev. B* **2010**, *82*, 205402. [CrossRef]
40. Xia, C.; Watcharinyanon, S.; Zakharov, A.A.; Yakimova, R.; Hultman, L.; Johansson, L.J.; Virojanadara, C. Si intercalation/deintercalation of graphene on 6H-SiC(0001). *Phys. Rev. B* **2012**, *85*, 045418. [CrossRef]
41. Emtsev, K.V.; Zakharov, A.A.; Coletti, C.; Forti, S.; Starke, U. Ambipolar doping in quasifree epitaxial graphene on SiC(0001) controlled by Ge intercalation. *Phys. Rev. B* **2011**, *84*, 125423. [CrossRef]
42. Chen, W.; Chen, S.; Ni, Z.H.; Huang, H.; Qi, D.C.; Gao, X.Y.; Shen, Z.X.; Wee, A.T.S. Band-Bending at the Graphene–SiC Interfaces: Effect of the Substrate. *Jpn. J. Appl. Phys.* **2010**, *49*, 01AH05. [CrossRef]
43. Tejeda, A.; Taleb-Ibrahimi, A.; de Heer, W.; Berger, C.; Conrad, E.H. Electronic structure of epitaxial graphene grown on the C-face of SiC and its relation to the structure. *New J. Phys.* **2012**, *14*, 125007. [CrossRef]
44. Jayasekera, T.; Xu, S.; Kim, K.W.; Nardelli, M.B. Electronic properties of the graphene/6H-SiC(0001) interface: A first-principles study. *Phys. Rev. B* **2011**, *84*, 035442. [CrossRef]
45. Dharmaraj, P.; Justin Jesuraj, P.; Jeganathan, K. Tuning a Schottky barrier of epitaxial graphene/4H-SiC(0001) by hydrogen intercalation. *Appl. Phys. Lett.* **2016**, *108*, 051605. [CrossRef]
46. Hannon, J.B.; Copel, M.; Tromp, R.M. Direct Measurement of the Growth Mode of Graphene on SiC(0001) and SiC(0001). *Phys. Rev. Lett.* **2011**, *107*, 166101. [CrossRef] [PubMed]
47. Hertel, S.; Finkler, A.; Krieger, M.; Weber, H.B. Graphene Ohmic Contacts to n-type Silicon Carbide (0001). *Mater. Sci. Forum* **2015**, *821–823*, 933–936. [CrossRef]
48. Mammadov, S.; Ristein, J.; Krone, J.; Raidel, C.; Wanke, M.; Wiesmann, V.; Speck, F.; Seyller, T. Work function of graphene multilayers on SiC(0001). *2D Mater.* **2017**, *4*, 015043. [CrossRef]
49. Tomer, D.; Rajput, S.; Hudy, L.J.; Li, C.H.; Li, L. Tuning a Schottky barrier of epitaxial graphene/4H-SiC(0001) by hydrogen intercalation. *Appl. Phys. Lett.* **2014**, *105*, 021607. [CrossRef]
50. Zhong, H.; Xu, K.; Liu, Z.; Xu, G.; Shi, L.; Fan, Y.; Wang, J.; Ren, G.; Yang, H. Charge transport mechanisms of graphene/semiconductor Schottky barriers: A theoretical and experimental study. *J. Appl. Phys.* **2014**, *115*, 013701. [CrossRef]
51. Rajput, S.; Chen, M.X.; Liu, Y.; Li, Y.Y.; Weinert, M.; Li, L. Spatial fluctuations in barrier height at the graphene-silicon carbide Schottky junction. *Nat. Commun.* **2013**, *4*, 2752. [CrossRef] [PubMed]
52. Seyller, T.; Emtsev, K.V.; Speck, F.; Gao, K.-Y.; Ley, L. Schottky barrier between 6H-SiC and graphite: Implications for metal/SiC contact formation. *Appl. Phys. Lett.* **2006**, *88*, 242103. [CrossRef]
53. Shivaraman, S.; Herman, L.H.; Rana, F.; Park, J.; Spencer, M.G. Schottky barrier inhomogeneities at the interface of few layer epitaxial graphene and silicon carbide. *Appl. Phys. Lett.* **2012**, *100*, 183112. [CrossRef]
54. Sonde, S.; Giannazzo, F.; Raineri, V.; Rimini, E. Investigation of graphene–SiC interface by nanoscale electrical characterization. *Phys. Status Solidi B* **2010**, *247*, 912–915. [CrossRef]
55. Yakimova, R.; Iakimov, T.; Syväjärvi, M. Process for Growth of Graphene. U.S. Patent US9150417B2, 6 October 2015.
56. Yager, T.; Lartsev, A.; Yakimova, R.; Lara-Avila, S.; Kubatkin, S. Wafer-scale homogeneity of transport properties in epitaxial graphene on SiC. *Carbon* **2015**, *87*, 409–414. [CrossRef]
57. Eriksson, J.; Pearce, R.; Iakimov, T.; Virojanadara, C.; Gogova, D.; Andersson, M.; Syväjärvi, M.; Lloyd Spetz, A.; Yakimova, R. The influence of substrate morphology on thickness uniformity and unintentional doping of epitaxial graphene on SiC. *Appl. Phys. Lett.* **2012**, *100*, 241607. [CrossRef]

58. Yazdi, G.; Vasiliauskas, R.; Iakimov, T.; Zakharov, A.; Syväjärvi, M.; Yakimova, R. Growth of large area monolayer graphene on 3C-SiC and a comparison with other SiC polytypes. *Carbon* **2013**, *57*, 477. [CrossRef]
59. Virojanadara, C.; Syväjarvi, M.; Yakimova, R.; Johansson, L.; Zakharov, A.; Balasubramanian, T. Homogeneous large-area graphene layer growth on 6H-SiC(0001). *Phys. Rev. B* **2008**, *78*, 1. [CrossRef]
60. Butt, N.Z.; Sarker, B.K.; Chen, Y.P.; Alam, M.A. Substrate-Induced Photofield Effect in Graphene Phototransistors. *IEEE Trans. Electron. Devices* **2015**, *62*, 3734. [CrossRef]
61. Anderson, T.J.; Hobart, K.D.; Greenlee, J.D.; Shahin, D.I.; Koehler, A.D.; Tadjer, M.J.; Imhoff, E.A.; Myers-Ward, R.L.; Christou, A.; Kub, F.J. Ultraviolet detector based on graphene/SiC heterojunction. *Appl. Phys. Express* **2015**, *8*, 041301. [CrossRef]
62. Sze, S.M.; Ng, K.K. *Physics of Semiconductor Devices*, 3rd ed.; Wiley: New York, NJ, USA, 2007; pp. 127–172.
63. Cumpson, P.J.; Seah, M.P. Elastic Scattering Corrections in AES and XPS. II. Estimating Attenuation Lengths and Conditions Required for their Valid Use in Overlayer/Substrate Experiments. *Surf. Interface Anal.* **1997**, *25*, 430. [CrossRef]
64. Johansson, L.I.; Owman, F.; Mårtensson, P. High-resolution core-level study of 6H-SiC(0001). *Phys. Rev. B* **1996**, *53*, 13793. [CrossRef]
65. Tadjer, M.J.; Anderson, T.J.; Hobart, K.D.; Nyakiti, L.O.; Wheeler, V.D.; Myers-Ward, R.L.; Gaskill, D.K.; Eddy, C.R., Jr.; Kub, F.J.; Calle, F. Vertical conduction mechanism of the epitaxial graphene/n-type 4H-SiC heterojunction at cryogenic temperatures. *Appl. Phys. Lett.* **2012**, *100*, 193506. [CrossRef]
66. Dharmaraj, P.; Jeganathan, K.; Parthiban, S.; Kwon, J.Y.; Gautam, S.; Chae, K.H.; Asokan, K. Selective area growth of Bernal bilayer epitaxial graphene on 4H-SiC(0001) substrate by electron-beam irradiation. *Appl. Phys. Lett.* **2014**, *105*, 181601. [CrossRef]
67. Tongay, S.; Lemaitre, M.; Miao, X.; Gila, B.; Appleton, B.R.; Hebard, A.F. Rectification at Graphene-Semiconductor Interfaces: Zero-Gap Semiconductor-Based Diodes. *Phys. Rev. X* **2012**, *2*, 011002. [CrossRef]
68. Giannazzo, F.; Hertel, S.; Albert, A.; La Magna, A.; Roccaforte, F.; Krieger, M.; Weber, H.B. Electrical Nanocharacterization of Epitaxial Graphene/Silicon Carbide Schottky Contacts. *Mater. Sci. Forum.* **2014**, *778–780*, 1142–1145. [CrossRef]
69. Tongay, S.; Schumann, T.; Hebard, A.F. Graphite based Schottky diodes formed on Si, GaAs, and 4H-SiC substrates. *Appl. Phys. Lett.* **2009**, *95*, 222103. [CrossRef]
70. Shtepliuk, I.; Khranovskyy, V.; Yakimova, R. Combining graphene with silicon carbide: Synthesis and properties—A review. *Semicond. Sci. Technol.* **2016**, *31*, 113004. [CrossRef]